

Altermagnetic superconducting diode effect

Sayan Banerjee¹ and Mathias S. Scheurer¹

¹*Institute for Theoretical Physics III, University of Stuttgart, 70550 Stuttgart, Germany*

Non-reciprocal superconductivity, also known as the superconducting diode effect, has been extensively studied in the presence of a magnetic field or some form of ferromagnetic order breaking time-reversal symmetry. We here show that another class of magnetic order known as altermagnetism, which also breaks time-reversal symmetry but does not exhibit a finite net magnetic moment, can also give rise to a superconducting diode effect. Whether this is the case depends on the combination of the system's point group and altermagnetic order parameter which we explore systematically for two-dimensional crystalline systems. If the superconducting electrons are in a centrosymmetric crystalline environment, an electric field E_z (or other sources of inversion symmetry breaking) can be used to turn on and tune the non-reciprocity, yielding an electric-field tunable diode effect; there are also non-centrosymmetric point groups, which are not reached by applying $E_z \neq 0$ in a centrosymmetric crystal, but still allow for an altermagnetic order parameter with non-reciprocal superconductivity. Depending on the residual magnetic point group, the zeros of the critical current asymmetry, $J_c(\hat{n}) - J_c(-\hat{n})$, are pinned along high-symmetry crystalline directions $\hat{n} = \hat{e}_j$ or are free to rotate in the plane of the system. In some cases, the zeros can be rotated by tuning the electric field E_z . We discuss all of these phenomena both on the general level using exact symmetry arguments and more explicitly by constructing and solving minimal lattice models. We provide experimental setups to realize the altermagnetic superconducting diode effect.

I. INTRODUCTION

The broad class of magnetically ordered states referred to as “altermagnets” (AMs) has recently become a subject of notable interest and has motivated a significant amount of theoretical [1–40] and experimental [41–47] studies, probing into its nature and emergence. Just as with any form of magnetic order, time-reversal symmetry is broken in an AM. However, as opposed to ferromagnets, AMs do not exhibit a finite net magnetic moment, which is guaranteed by a magnetic point symmetry. This means that the state is invariant under the product Θg_m of time-reversal Θ and a unitary lattice symmetry g_m . Unlike a collinear antiferromagnet, g_m is not lattice translation for an AM, where the reversal of all local magnet moments resulting from application of Θ cannot be undone by a lattice translation $T_{\mathbf{R}}$. Instead, g_m is a point group symmetry such as a rotation or reflection symmetry of the underlying crystalline lattice.

While a Pomeranchuk instability [48, 49] in the $l = 2$ (or higher l) spin-triplet channel of a Fermi liquid falls into the category of AMs, a lot of interesting novel consequences have recently been uncovered. For instance, since g_m is not translation, AMs can exhibit an anomalous Hall effect, even without net magnetic moment, unlike antiferromagnets where $\Theta T_{\mathbf{R}}$ does not allow for a finite Hall response [11, 46]. Furthermore, the spin texture of the Bloch states in the presence of an AM can lead to a Zeeman splitting with protected nodal lines [29]. Further consequences have been explored in thermal transport [28], in Josephson junctions [14, 27], and other tunnel junction setups [50]. What is more, the effect of AMs on other coexisting interaction-induced orders is very rich;

in particular, superconductivity [18, 31–36, 39, 51] has been explored, sparking off broader questions regarding the nature of strongly correlated materials exhibiting superconductivity and magnetism beyond the conventional paradigm of ferromagnetism and antiferromagnetism.

Concurrently, non-reciprocal transport in superconductors and superconducting junctions, particularly the superconducting diode effect (SDE), has garnered various experimental [52–78] and theoretical [79–114] attention. The SDE refers to a difference in the critical current $J_c(\hat{n})$ in opposite directions, \hat{n} and $-\hat{n}$. In that case, applying a current J with $\min(J_c(\pm\hat{n})) < J < \max(J_c(\pm\hat{n}))$, leads to superconducting transport along one and resistive behavior along the opposite direction, yielding a superconducting analogue of a semi-conducting diode. On top of fundamental theoretical questions, the rich space of potential applicability of such non-reciprocal responses on modern-day electronics and devices renders the SDE an exciting topic to delve into from an experimental and technological standpoint.

Importantly, time-reversal symmetry Θ implies $J_c(\hat{n}) = J_c(-\hat{n})$ which therefore needs to be broken to obtain a finite SDE. So far, external magnetic fields [53–66, 68, 79–83, 87, 94–96, 103, 107, 110, 111], proximity-induced magnetism [72, 73, 76], and interaction-induced order parameters in the same electron liquid [74, 84, 109, 115] have been discussed as possible causes for the broken time-reversal symmetry inducing the SDE. All of these Θ -breaking orders fall under the category of (spin and/or orbital) ferromagnetism and are associated with a non-zero net magnetic moment. Due to its residual magnetic symmetry $\Theta T_{\mathbf{e}_{x,y}}$, with nearest-neighbor vectors $\mathbf{e}_{x,y}$, collinear antiferromagnetism as the only cause of symmetry reduction cannot stabilize the SDE. This

therefore begs the question if and under which conditions AMs can induce a SDE in an otherwise symmetry-unbroken superconductor and what the consequences are of the non-trivial magnetic point symmetries of the AM on the critical current $J_c(\hat{\mathbf{n}})$. This is the scope of our present work.

To this end, we here systematically analyze, using a combination of symmetry arguments and explicit model calculations, which of the possible AMs in two-dimensional (2D) crystalline systems can yield a critical current asymmetry $J_c(\hat{\mathbf{n}}) - J_c(-\hat{\mathbf{n}}) \neq 0$. Indeed, there are several candidate AMs where a SDE is possible despite the lack of net magnetization. We will show that, depending on the residual magnetic point group, the zeros of the current asymmetry $J_c(\hat{\mathbf{n}}) - J_c(-\hat{\mathbf{n}})$ are either aligned with high-symmetry crystalline directions, can be rotated by an electric field, or are not at all pinned to the crystalline axes.

The remainder of the manuscript is organized as follows. In Sec. II, we describe the method of calculating $J_c(\hat{\mathbf{n}})$ and discuss the general constraints on its directional dependence and on its asymmetry resulting from magnetic point symmetries. We further systematically go through all AM order parameters in 2D single-band models, study whether they induce an SDE and, if so, how the current asymmetry $J_c(\hat{\mathbf{n}}) - J_c(-\hat{\mathbf{n}})$ depends on $\hat{\mathbf{n}}$. In Sec. III, we demonstrate the AM-induced SDE on a case-by-case basis by constructing and solving explicit lattice models, detailing the distinctive characters in each of the cases. Finally, Sec. IV summarizes our findings.

II. GENERAL CONSIDERATIONS

Before presenting explicit calculations, we start by discussing general constraints on the AM-induced SDE, resulting from symmetries. We will see under which conditions the SDE is forced to vanish along high-symmetry directions and systematically go through all possible AM order parameters of 2D systems.

A. Diode effect efficiency

To set the stage for our symmetry discussion, we begin by first outlining the basic procedure for the calculation of the critical current. Denoting the superconducting order parameter for Cooper pairs with center-of-mass momentum \mathbf{q} by $\Delta_{\mathbf{q}}$, we expand the change of the free-energy as a result of superconductivity $\delta\mathcal{F}_S := \mathcal{F}[\Delta_{\mathbf{q}}] - \mathcal{F}[0]$ up to quartic order in $\Delta_{\mathbf{q}}$,

$$\delta\mathcal{F}_S \sim \sum_{\mathbf{q}} a_{\mathbf{q}}^S |\Delta_{\mathbf{q}}|^2 + b^S \sum_{\mathbf{q}_i} \Delta_{\mathbf{q}_1}^* \Delta_{\mathbf{q}_2}^* \Delta_{\mathbf{q}_3} \Delta_{\mathbf{q}_4} \delta_{\mathbf{q}_1+\mathbf{q}_2, \mathbf{q}_3+\mathbf{q}_4}, \quad (1)$$

where we neglected the momentum dependence of the quartic term. The equilibrium superconducting state is found by minimizing $\delta\mathcal{F}_S$. Restricting the analysis to single- \mathbf{q} states, $\Delta_{\mathbf{q}} \propto \delta_{\mathbf{q}, \mathbf{q}_0}$, the value of \mathbf{q}_0 is determined by the minimum of $a_{\mathbf{q}}^S$. We define the critical current $J_c(\hat{\mathbf{n}})$ along $\hat{\mathbf{n}}$ as the maximal magnitude of $\mathbf{J}(\mathbf{q}) = 2e\Delta_{\mathbf{q}}\nabla a_{\mathbf{q}}^S$ oriented along $\hat{\mathbf{n}}$. Postponing a microscopic evaluation of $a_{\mathbf{q}}^S$ to Sec. III below, we here only note that a unitary symmetry with vector representation g implies $a_{\mathbf{q}}^S = a_{g\mathbf{q}}^S$ and, thus, $\mathbf{J}(g\mathbf{q}) = g\mathbf{J}(\mathbf{q})$ as well as $J_c(\hat{\mathbf{n}}) = J_c(g\hat{\mathbf{n}})$.

To quantify the ‘degree’ or amount of diode effect, it will be convenient for us to first introduce a signed efficiency parameter

$$\eta_s(\hat{\mathbf{n}}) := \frac{J_c(\hat{\mathbf{n}}) - J_c(-\hat{\mathbf{n}})}{J_c(\hat{\mathbf{n}}) + J_c(-\hat{\mathbf{n}})} \quad (2)$$

such that the angle-resolved diode-effect efficiency is $\eta(\hat{\mathbf{n}}) = |\eta_s(\hat{\mathbf{n}})| \geq 0$. We next discuss symmetry constraints on $\eta(\hat{\mathbf{n}})$. From the discussion above, it follows that a unitary symmetry with vector representation g enforces $\eta_s(g\hat{\mathbf{n}}) = \eta_s(\hat{\mathbf{n}})$. Since $\eta_s(\hat{\mathbf{n}}) = -\eta_s(-\hat{\mathbf{n}})$, which immediately follows from the definition (2), the SDE efficiency is required to vanish along any direction $\hat{\mathbf{n}}_0$ obeying $g\hat{\mathbf{n}}_0 = -\hat{\mathbf{n}}_0$; in short:

$$g\hat{\mathbf{n}}_0 = -\hat{\mathbf{n}}_0 \quad \Rightarrow \quad \eta(\hat{\mathbf{n}}_0) = 0. \quad (3)$$

Clearly, Eq. (3) is obeyed for all $\hat{\mathbf{n}}$ if g is inversion (I) or two-fold rotation along the out-of-plane ($\hat{\mathbf{z}}$) direction C_{2z} for a 2D system; these symmetries are thus required to be broken to allow for a finite SDE. While the following constraints are readily generalized to three spatial dimensions, we first focus for notational simplicity on a 2D system in the xy plane. If g is a two-fold rotational symmetry, $C_{2\hat{\mathbf{m}}}$, along an in-plane direction $\hat{\mathbf{m}}$ or a mirror-plane symmetry, $\sigma_{\hat{\mathbf{m}}}$, spanned by $\hat{\mathbf{z}}$ and $\hat{\mathbf{m}}$, Eq. (3) implies that $\eta(\hat{\mathbf{n}}) = 0$ for $\hat{\mathbf{n}}$ perpendicular to $\hat{\mathbf{m}}$. In other words, the zeros of $\eta(\hat{\mathbf{n}})$ are pinned along high-symmetry directions if the point group contains two-fold rotations along in-plane directions or mirror planes perpendicular to the system plane. Note that rotations with degrees higher than two do not pin the zeros.

Similar constraints arise from magnetic point symmetries, i.e., non-unitary symmetries, Θg_m , given by the product of time-reversal Θ and some unitary symmetry g_m . Such a magnetic symmetry implies $a_{\mathbf{q}}^S = a_{-g_m\mathbf{q}}^S$ and consequently $J_c(\hat{\mathbf{n}}) = J_c(-g_m\hat{\mathbf{n}})$; this, in turn, leads to $\eta_s(g_m\hat{\mathbf{n}}) = \eta_s(-\hat{\mathbf{n}}) = -\eta_s(\hat{\mathbf{n}})$. As such, the presence of the magnetic symmetry Θg_m implies that

$$g_m\hat{\mathbf{n}}_0 = \hat{\mathbf{n}}_0 \quad \Rightarrow \quad \eta(\hat{\mathbf{n}}_0) = 0. \quad (4)$$

Equation (4) contains the special case of preserved time-reversal symmetry, $g_m = \mathbb{1}$ for which $g_m\hat{\mathbf{n}} = \hat{\mathbf{n}}$ always holds, implying $\eta(\hat{\mathbf{n}}) = 0$ for all $\hat{\mathbf{n}}$; this just recovers the often-stated fact that Θ needs to be broken to

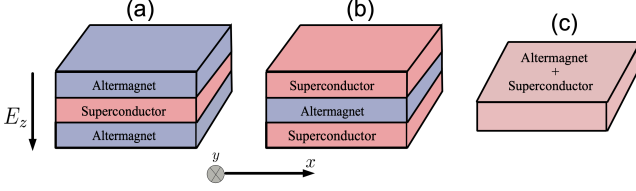


FIG. 1: Schematic of the possible realizations of the considered models by (a) proximity-induced AM in a superconductor, (b) proximity-induced superconductivity on an AM metal, and (c) both orders coexisting in a single material. Our analysis also applies to the case where the proximitizing material, the AM in (a) and the superconductor in (b), is only present on one side. The advantage of the symmetric design is that an external electric field E_z can be used to reduce the symmetries of the systems in a controllable way.

get a SDE. However, Eq. (4) also shows that zeros of the angle-resolved SDE efficiency are pinned along high-symmetry directions if the system exhibits a magnetic reflection symmetry, $\Theta\sigma_{\hat{m}}$, or magnetic rotational symmetry, $\Theta C_{2\hat{m}}$; in both cases, it holds $\eta(\hat{n}) = 0$. We will see examples of all of these constraints in the explicit model calculations of Sec. III below.

We finally point out that Eqs. (3) and (4) also apply for the three-dimensional case. As such, we see that a two-fold non-magnetic rotation (mirror) symmetry lead to line (point) nodes for $\eta(\hat{n})$ on the sphere $\{\hat{n} \in \mathbb{R}^3 | \hat{n}^2 = 1\}$, while magnetic rotations (mirror) symmetries imply point (line) nodes.

B. AM-induced SDE

With these symmetry constraints at hand, we are now in position to analyze under which conditions an AM moment can induce a SDE and, if non-zero, whether the angle-resolved SDE efficiency $\eta(\hat{n})$ has to have zeros along certain directions. To be precise, in this work, we use the following definition of an AM order parameter. We define an AM order parameter as a time-reversal-odd order parameter (i.e., some form of magnetic order), which unlike a ferromagnet does not lead to a finite net magnetic moment or spin-polarization; in addition, we require that it preserve lattice translation, unlike an antiferromagnet or more complex translational-symmetry-breaking orders (such as an incommensurate spiral or a tetrahedral magnet).

For concreteness, we study the prototypical case of a minimal model for the normal state—one that only contains a single, spinful band,

$$\mathcal{H}_0 = \sum_{\mathbf{k}} c_{\mathbf{k},s}^\dagger [s_0 \epsilon_{\mathbf{k}} + \mathbf{g}_{\mathbf{k}} \cdot \mathbf{s} + \mathbf{N}_{\mathbf{k}} \cdot \mathbf{s}]_{s,s'} c_{\mathbf{k},s'}, \quad (5)$$

where $c_{\mathbf{k},s}^\dagger$ are electron creation operators of spin s and momentum \mathbf{k} , $\mathbf{s} = (s_x, s_y, s_z)$, $s_0 = \mathbb{1}$, are spin Pauli matrices. Furthermore, $\epsilon_{\mathbf{k}}$ is the bare dispersion, $\mathbf{g}_{\mathbf{k}}$ the spin-orbit vector, and $\mathbf{N}_{\mathbf{k}}$ the AM order parameter. Since these three quantities are, by design, even, even, and odd under Θ , respectively, they have to obey

$$\epsilon_{\mathbf{k}} = \epsilon_{-\mathbf{k}}, \quad \mathbf{g}_{\mathbf{k}} = -\mathbf{g}_{-\mathbf{k}}, \quad \mathbf{N}_{\mathbf{k}} = \mathbf{N}_{-\mathbf{k}}. \quad (6)$$

We, therefore, conclude that $\epsilon_{\mathbf{k}}$ always preserves inversion, $\mathbf{g}_{\mathbf{k}}$ can only be non-zero if inversion, I , is broken (as usual), and the AM order parameter cannot break I (and will always be odd under ΘI) in the class of models in Eq. (5). To describe superconductivity, we assume that Cooper pairs form in the spin-singlet channel, the superconducting order parameter transforms trivially under all point symmetries and preserves time-reversal. Therefore, $\mathbf{N}_{\mathbf{k}}$ is the only term breaking time-reversal and $\mathbf{g}_{\mathbf{k}}$ the only source of broken inversion symmetry in Eq. (5); this is why both are required to obtain a finite SDE, $\eta \neq 0$.

The different possible physical realizations of this class of models are illustrated in Fig. 1. Either the AM term $\mathbf{N}_{\mathbf{k}}$ will be proximity-induced in superconducting systems, see Fig. 1(a), or vice versa—a proximitized superconductor induces pairing in a metallic AM material [Fig. 1(b)]. Although not essential for the realization of the following effects, we here assumed that the proximitizing materials are placed symmetrically on both sides such that an electric field, E_z , can be used to further reduce the symmetries *in situ*. Our symmetry analysis and minimal-model study here still applies when the proximitizing material is only present on one side. In that case, the terms induced by $E_z \neq 0$ in the models below will already be present for $E_z = 0$. Finally, our analysis also applies if both AM and superconductivity arise spontaneously in the same electron liquid, see Fig. 1(c). We note in passing that this is the only scenario which would allow to realize altermagnetic diodes as a bulk effect in three dimensions and where the backaction mechanism of Ref. 115 can apply, possibly giving rise to enhanced η .

To address the question which AM order parameters can induce a SDE, we start by considering all possible point groups \mathcal{G}_0 of 2D crystalline systems. For each of them, we go through all of its irreducible representations and check whether a generic time-reversal-odd $\mathbf{N}_{\mathbf{k}} \cdot \mathbf{s}$ in Eq. (5) transforming under it is an AM; this requires the presence of a residual symmetry that ensures that the expectation value of the total spin,

$$\mathbf{S} = \sum_{\mathbf{k}} c_{\mathbf{k},s}^\dagger \mathbf{s}_{s,s'} c_{\mathbf{k},s'}, \quad (7)$$

has to vanish. For instance, an AM order parameter transforming under A_g of $\mathcal{G}_0 = D_{2h}$ will lead to a residual C_{2z} rotation symmetry, implying that $\langle S_x \rangle = \langle S_y \rangle = 0$. The additional σ_v mirror symmetry further implies that also $\langle S_z \rangle$ vanishes. In the first three columns of Table I,

we list all such combinations of \mathcal{G}_0 and AM order parameters, some of which were already tabulated in Ref. 29. To organize the list, the first 11 lines refer to the AM order parameters for centrosymmetric point groups \mathcal{G}_0 ; interestingly, we find that, in all cases, these AM order parameters will continue to be proper AMs with $\langle \mathbf{S} \rangle = 0$ when an electric field is applied, $E_z \neq 0$, which reduces the point groups to $\mathcal{G}_{E_z} \leq \mathcal{G}_0$. Coming back to our previous example, $\mathcal{G}_0 = D_{2h}$ will be reduced to $\mathcal{G}_{E_z} = C_{2v}$. It still contains the two symmetries used above to show that there is no finite magnetization. The remaining lines of Table I refer to the AM order parameters in the 2D non-centrosymmetric point groups that are not reached by applying E_z in centrosymmetric point groups. In all those cases, reducing the point group further by application of E_z leads to a finite magnetization.

For all of these AMs and point groups, we investigate whether a superconducting order parameter in the singlet channel and transforming under the trivial representation of \mathcal{G}_0 can give rise to a SDE. Clearly, due to inversion symmetry, there cannot be a SDE for the centrosymmetric point groups at $E_z = 0$. However, applying an electric field does allow for finite η in a few cases, see penultimate column in Table I. This is remarkable since it shows that finite magnetization is not required to obtain a SDE. Also some of the AMs in certain non-centrosymmetric point groups allow for a SDE without finite moment. In Table I we also list whether and, if so, how the residual symmetries pin the zeros of $\eta(\hat{\mathbf{n}})$ to high-symmetry lines. These aspects will be further discussed on a case-by-case basis in the following section.

III. MODEL STUDIES

In order to demonstrate the features we have deduced by symmetry analysis above more explicitly and to discuss additional aspects, we here construct and solve concrete lattice models; to this end, we use three different point groups and AM order parameters that can induce an SDE as examples.

A. General formalism

In all of these lattice models, superconductivity will be described in the same way. We start with an attractive ($g > 0$) interaction in the spin-singlet Cooper channel,

$$\mathcal{H}_I = -g \sum_{\mathbf{q}} C_{\mathbf{q}}^\dagger C_{\mathbf{q}}, \quad C_{\mathbf{q}} = \sum_{\mathbf{k}} c_{\mathbf{k}+\mathbf{q}/2} i s_y c_{-\mathbf{k}+\mathbf{q}/2}, \quad (8)$$

and add it to the Hamiltonian in Eq. (5), $\mathcal{H}_0 \rightarrow \mathcal{H}_0 + \mathcal{H}_I$. We then perform a mean-field decoupling in the Cooper channel and introduce $\Delta_{\mathbf{q}} = g \langle C_{\mathbf{q}} \rangle$, leading to

the following Hamiltonian

$$\begin{aligned} \mathcal{H}_{\text{MF}} = & \sum_{\mathbf{k}} c_{\mathbf{k}}^\dagger h_{\mathbf{k}} c_{\mathbf{k}} + \sum_{\mathbf{k}, \mathbf{q}} \left[\Delta_{\mathbf{q}} c_{\mathbf{k}+\mathbf{q}/2}^\dagger i s_y c_{-\mathbf{k}+\mathbf{q}/2}^\dagger + \text{H.c.} \right] \\ & + \sum_{\mathbf{q}} \frac{|\Delta_{\mathbf{q}}|^2}{g}, \quad h_{\mathbf{k}} = s_0 \epsilon_{\mathbf{k}} + \mathbf{g}_{\mathbf{k}} \cdot \mathbf{s} + \mathbf{N}_{\mathbf{k}} \cdot \mathbf{s}. \end{aligned} \quad (9)$$

Using a redundant Nambu basis, defined by $\Psi_{\mathbf{k}} = (c_{\mathbf{k}+\mathbf{q}/2}, i s_y c_{-\mathbf{k}+\mathbf{q}/2}^\dagger)^T$, we obtain a Bogoliubov-de Gennes Hamiltonian,

$$H_{\text{BdG}} = \begin{pmatrix} h_{\mathbf{k}+\mathbf{q}/2} & \Delta_{\mathbf{q}} \\ \Delta_{\mathbf{q}}^* & -s_y h_{-\mathbf{k}+\mathbf{q}/2}^* s_y \end{pmatrix} \quad (10)$$

which allows us to rewrite the Hamiltonian (9) for a given \mathbf{q} as,

$$\mathcal{H}_{\text{MF}}(\mathbf{q}) = \sum_{\mathbf{k}} \Psi_{\mathbf{k}}^\dagger H_{\text{BdG}} \Psi_{\mathbf{k}} + \frac{|\Delta_{\mathbf{q}}|^2}{g}. \quad (11)$$

Next, we integrate out the electrons in this quadratic mean-field Hamiltonian and recover the Ginzburg-Landau expression in Eq. (1). The key quantity $a_{\mathbf{q}}^S$ is related to the particle-particle bubble $\Gamma(\mathbf{q})$ at finite \mathbf{q} in the usual way, $a_{\mathbf{q}}^S = g^{-1} - \Gamma(\mathbf{q})$. Keeping both intra- and inter-band contributions, the particle-particle bubble is of the form

$$\Gamma(\mathbf{q}) = \frac{1}{4} \sum_{\mathbf{k}, \nu=p, m, \eta=\pm} \Lambda_{\mathbf{k}, \mathbf{q}, \nu, \eta} \tanh \frac{\mathcal{E}_{\mathbf{k}, \mathbf{q}, \nu, \eta}}{2T}, \quad (12)$$

where $\Lambda_{\mathbf{k}, \mathbf{q}, \nu, \eta}$ contains the coherence factors and $\mathcal{E}_{\mathbf{k}, \mathbf{q}, \nu, \eta}$ are Bogoliubov energies (see Appendix B for their explicit form); the indices ν and μ label the four different states associated with spin and particle-hole space in our redundant Nambu basis, cf. Eq. (10). From the resulting $a_{\mathbf{q}}^S$, we compute the directional dependence of the critical current and hence $\eta(\hat{\mathbf{n}})$ as described in Sec. II A. We will next apply this formalism using a few different normal-state Hamiltonians, \mathcal{H}_0 , to elucidate the nature of the SDE in various point groups.

B. Pinned zeros and E_z tunability in D_{6h}

We start from the centrosymmetric point group $\mathcal{G}_0 = D_{6h}$, where $\epsilon_{\mathbf{k}}$ obeys $\epsilon_{\mathbf{k}} = \epsilon_{-\mathbf{k}} = \epsilon_{C_{3z}\mathbf{k}} = \epsilon_{\sigma_v\mathbf{k}}$. To model such a dispersion, we take a nearest-neighbor hopping model on the triangular lattice, $\epsilon_{\mathbf{k}} = -\sum_{j=1}^3 t \cos(\mathbf{a}_j \cdot \mathbf{k})$, where \mathbf{a}_j are three C_{3z} -related primitive vectors. For notational simplicity, we measure all energies in units of t in the following. The presence of I in D_{6h} implies $\mathbf{g}_{\mathbf{k}} = 0$. We can see in Table I that D_{6h} has four possible AM order parameters and only two of them—those transforming under B_{1g} and B_{2g} —can give rise to a SDE

TABLE I: Summary of possible AM order parameters $\mathbf{N}_{\mathbf{k}}$ in 2D models of the form of Eq. (5). For each point group \mathcal{G}_0 , we list all the irreducible representations (IR) that can give rise to an AM; the respective form of $\mathbf{N}_{\mathbf{k}}$ for small \mathbf{k} is shown in the third column, where τ and R_φ are, respectively, a real-valued constant and a rotation matrix along the third direction not fixed by symmetry. Applying an electric field E_z reduces the point group to \mathcal{G}_{E_z} . In case of the centrosymmetric \mathcal{G}_0 (first 11 lines), all order parameters remain AMs (as indicated in the fourth column), characterized by zero net magnetization; this is not the case for the non-centrosymmetric \mathcal{G}_0 (line 12-20). In the column SDE, we indicate whether the respective AM will give rise to an SDE (in the centrosymmetric point groups, only possible for $E_z \neq 0$). We also indicate whether the angle-resolved SDE efficiency $\eta(\hat{\mathbf{n}})$ has zeros along generic directions $\hat{\mathbf{n}}_0$ (and their C_{3z} -related partners) or along crystalline axes, $\hat{\mathbf{e}}_{x,y}$. For D_3 and D_6 , we introduced $\hat{\mathbf{n}}_{E_z}^i$ with $\hat{\mathbf{n}}_{E_z=0}^i = \hat{\mathbf{e}}_i$, $i = x, y$, and pointing along a generic direction for $E_z \neq 0$. The last column shows candidate materials, based on their conduction type—metallic (M) or insulating (I)—focusing on those cases where an SDE is present.

\mathcal{G}_0	IR of AM	$\mathbf{N}_{\mathbf{k}}$	\mathcal{G}_{E_z}	SDE	Materials
C_{4h}	B_g	$(0, 0, k_x^2 - k_y^2 + \tau k_x k_y)$	C_4 ; AM	\mathbf{x}	
C_{6h}	B_g	$R_\varphi(k_x^2 - k_y^2, -2k_x k_y, 0)$	C_6 ; AM	$\eta(\pm C_{3z}^j \hat{\mathbf{n}}_0) = 0$	
D_{2h}	A_g	$(0, 0, k_x k_y)$	C_{2v} ; AM	\mathbf{x}	
D_{4h}	A_{1g}	$(0, 0, k_x k_y (k_x^2 - k_y^2))$	C_{4v} ; AM	\mathbf{x}	
	B_{1g}	$(0, 0, k_x k_y)$		\mathbf{x}	
	B_{2g}	$(0, 0, k_x^2 - k_y^2)$		\mathbf{x}	
D_{6h}	A_{1g}	$(0, 0, k_x k_y (k_x^2 - 3k_y^2)(3k_x^2 - k_y^2))$	C_{6v} ; AM	\mathbf{x}	
	B_{1g}	$(k_x^2 - k_y^2, -2k_x k_y, 0)$		$\eta(\pm C_{3z}^j \hat{\mathbf{e}}_x) = 0$	CrSb (M)[2], MnTe (I)[116, 117]
	B_{2g}	$(2k_x k_y, k_x^2 - k_y^2, 0)$		$\eta(\pm C_{3z}^j \hat{\mathbf{e}}_y) = 0$	
	E_{2g}	$(0, 0, 2k_x k_y), (0, 0, k_x^2 - k_y^2)$		\mathbf{x}	
D_{3d}	A_{1g}	$(k_x^2 - k_y^2, -2k_x k_y, \tau k_x k_y (k_x^2 - 3k_y^2)(k_y^2 - 3k_x^2))$	C_{3v} ; AM	$\eta(\pm C_{3z}^j \hat{\mathbf{e}}_y) = 0$	Fe ₂ O ₃ , CoF ₃ (I) [2]
D_2	A	$(0, 0, k_x k_y)$	C_2 ; no AM	\mathbf{x}	
D_3	A_1	$(k_x^2 - k_y^2, -2k_x k_y, \tau k_x k_y (k_x^2 - 3k_y^2)(k_y^2 - 3k_x^2))$	C_3 ; no AM	$\eta(\pm C_{3z}^j \hat{\mathbf{n}}_{E_z}^y) = 0$	
D_4	A_1	$(0, 0, k_x k_y (k_x^2 - k_y^2))$	C_4 ; no AM	\mathbf{x}	
	B_1	$(0, 0, k_x k_y)$		\mathbf{x}	
	B_2	$(0, 0, k_x^2 - k_y^2)$		\mathbf{x}	
D_6	A_1	$(0, 0, k_x k_y (k_x^2 - 3k_y^2)(3k_x^2 - k_y^2))$	C_6 ; no AM	\mathbf{x}	
	B_1	$(k_x^2 - k_y^2, -2k_x k_y, 0)$		$\eta(\pm C_{3z}^j \hat{\mathbf{n}}_{E_z}^y) = 0$	VNB ₃ S ₆ (M)[2, 118]
	B_2	$(2k_x k_y, k_x^2 - k_y^2, 0)$		$\eta(\pm C_{3z}^j \hat{\mathbf{n}}_{E_z}^x) = 0$	
	E_2	$(0, 0, 2k_x k_y), (0, 0, k_x^2 - k_y^2)$		\mathbf{x}	

when also applying an electric field E_z . For concreteness, we will here focus on B_{1g} , which reduces D_{6h} to the magnetic point group generated by C_{3z} , ΘC_{2z} , $\Theta \sigma_v$, and I . We construct the lowest-order, Brillouin-zone-periodic form of $\mathbf{N}_{\mathbf{k}}$ consistent with B_{1g} , which corresponds to first-nearest-neighbor-hopping processes on the triangular lattice, with explicit form presented in Appendix B; it behaves as

$$\mathbf{N}_{\mathbf{k}} \sim N_0(k_x^2 - k_y^2, -2k_x k_y, 0)^T \quad (13)$$

around the Γ point, i.e., for $|\mathbf{k}| \rightarrow 0$. Due to $\mathbf{N}_{\mathbf{k}} = \mathbf{N}_{-\mathbf{k}}$, see Eq. (6), and B_{1g} being odd under C_{2z} , it holds $(\mathbf{N}_{\mathbf{k}})_z = 0$ to arbitrary order in \mathbf{k} . Note that this order parameter obeys all of the properties in our definition of an AM: by design [see Eq. (9)] it is translationally invariant and breaks time-reversal symmetry (due to $\mathbf{N}_{\mathbf{k}} = \mathbf{N}_{-\mathbf{k}}$). The absence of finite spin polarization immediately follows by noting that the residual C_{3z} and

$C_{2z}\Theta$ symmetries (also present for $E_z \neq 0$) imply, respectively, that $\langle S_{x,y} \rangle$ and $\langle S_z \rangle$ have to vanish, which we have also checked explicitly.

To understand the salient features of this model, let us start first with $E_z = 0$, with results displayed in the first column (a) of Fig. 2. One can see in Fig. 2(ai) and (aai) that the maximum of $\Gamma(\mathbf{q})$ is pinned to $\mathbf{q} = 0$ as long as N_0 in Eq. (13) is smaller than a critical value. This pinning is a consequence of C_{3z} symmetry. It means that, in the current model, a sufficiently strong AM order is required to induce finite-momentum pairing. While finite-momentum pairing can be induced by AM order, as pointed out in recent publications in the context of different models without C_{3z} symmetry [31, 51], it does not necessarily follow immediately, as we can see here. Moreover, since we have inversion symmetry and unbroken C_{3z} , we observe that $\Gamma(\mathbf{q})$ is six-fold symmetric. This symmetry is inherited by the critical current $J_c(\hat{\mathbf{n}})$ shown

in Fig. 2(aiii); it thus obeys $J_c(\hat{n}) = J_c(-\hat{n})$ and there is no SDE, $\eta = 0$, see Fig. 2(aiv).

As anticipated in Table I, we therefore have to apply an electric field E_z , which reduces D_{6h} to C_{6v} , to get an SDE. On the level of the Hamiltonian, the electric field induces a non-zero spin-orbit vector $\mathbf{g}_\mathbf{k}$. We again refer to Appendix B for its explicit form throughout the Brillouin zone and here only note that $\mathbf{g}_\mathbf{k} \sim \alpha(k_y, -k_x, 0)^T$ as $|\mathbf{k}| \rightarrow 0$. Similar to $(\mathbf{N}_\mathbf{k})_z = 0$ noted above, the last component $(\mathbf{g}_\mathbf{k})_z$ has to vanish to all orders in \mathbf{k} as a consequence of C_{2z} and Eq. (6).

The corresponding results for finite E_z are shown in the second column, (b), of Fig. 2. We observe that, even in the presence of $\alpha \neq 0$, the maximum of $\Gamma(\mathbf{q})$ is pinned to zero momentum, see Fig. 2(bi), due to the still unbroken C_{3z} symmetry. However, as a consequence of inversion symmetry breaking, $\Gamma(\mathbf{q})$ is not an even function anymore. As soon as a critical value of N_0 is surpassed, the maxima of $\Gamma(\mathbf{q})$ move from zero \mathbf{q} to three non-zero, C_{3z} -related momenta, as indicated by the orange circles in Fig. 2(bii). The number of degenerate maxima is reduced from six to three [compared with Fig. 2(aii)] when applying $E_z \neq 0$ as I is broken.

By the same token, the critical current $J_c(\hat{n})$ is not an even function anymore, see Fig. 2(biii), and we obtain a SDE, $\eta \neq 0$, as can be clearly seen in Fig. 2(biv). This demonstrates explicitly that a SDE is also possible when the only source of broken Θ is an AM, i.e., in the absence of a net magnetic moment. As the SDE requires broken I , it is tunable by an electric field. What is more, we observe that $\eta(\hat{n})$ has zeros along the high-symmetry directions \hat{e}_x , $C_{3z}\hat{e}_x$, and $C_{3z}^2\hat{e}_x$ as follows from the magnetic reflection symmetry $\Theta\sigma_v$ and Eq. (4) [or σ_d and Eq. (3) for that matter]. For an AM order parameter transforming under B_{2g} , the behavior is very similar. The main difference is that the aforementioned zeros of $\eta(\hat{n})$ are pinned along the orthogonal directions \hat{e}_y , $C_{3z}\hat{e}_y$, and $C_{3z}^2\hat{e}_y$, since, instead of $\Theta\sigma_v$, we have the magnetic reflection symmetry $\Theta\sigma_d$.

C. Generic zeros in C_{6h}

To demonstrate explicitly that the zeros of $\eta(\hat{n})$ are not always pinned along high-symmetry directions for the SDE induced by an AM, we next consider the case $\mathcal{G}_0 = C_{6h}$. It exhibits no rotations $C_{2\hat{m}}$ or reflections $\sigma_{\hat{m}}$ with in-plane \hat{m} , such that neither Eq. (3) nor Eq. (4) can apply (irrespective of the form of broken time-reversal symmetry). One consequence of the reduced symmetries is that the bare dispersion exhibits more terms compared to D_{6h} discussed above, which we describe with the

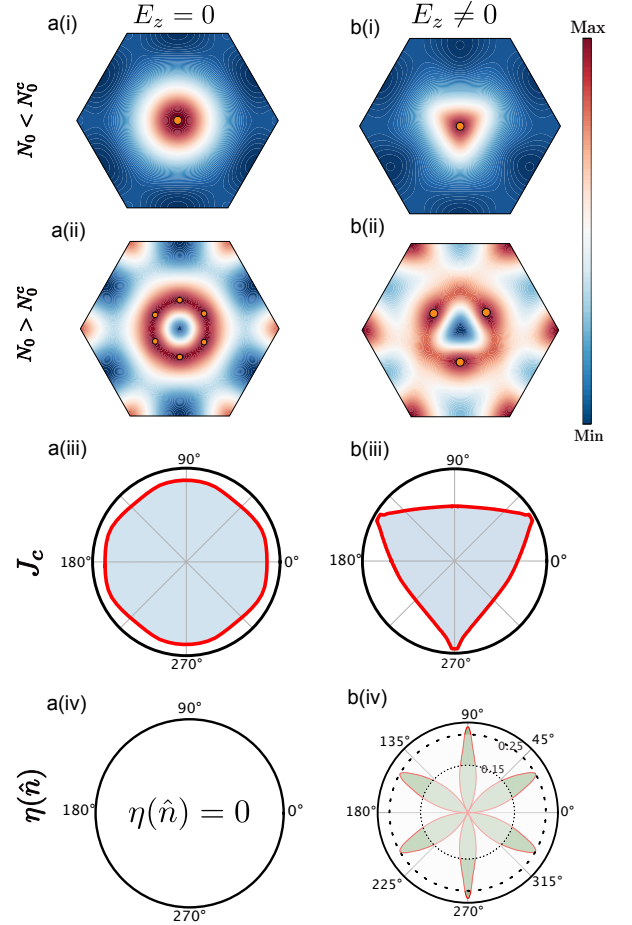


FIG. 2: SDE in point group D_{6h} . Column (a) and (b) compare the cases for zero and non-zero electric field E_z . Row (i) and (ii) show the particle-particle bubble $\Gamma(\mathbf{q})$ in the Brillouin zone below and above the critical value of the strength, N_0 , of the AM order; the orange circles denote the location of the maxima. Row (iii) shows the critical current $J_c(\hat{n})$ as a function of direction \hat{n} . The resulting angle-resolved SDE efficiency (2) is plotted in the last row (iv) and is only finite for $E_z \neq 0$. The magnetic point group dictates the zeros of η to be confined along high-symmetry directions, as discussed in the main text. Explicit parameters are given in [119].

leading-order contribution, $\propto t'$, in

$$\epsilon_{\mathbf{k}} = - \sum_{j=1}^3 (t \cos(\mathbf{a}_j \cdot \mathbf{k}) + t' \cos(\mathbf{a}'_j \cdot \mathbf{k})). \quad (14)$$

Here, \mathbf{a}'_j are three C_{3z} -related next-nearest-neighbor vectors on the triangular lattice ($\mathbf{a}'_1 = 2\mathbf{a}_2 - \mathbf{a}_1$, $\mathbf{a}'_j = C_{3z}^{j-1}\mathbf{a}'_1$). As can be seen in Table I, only one of the two possible AM order parameters—the one transforming under B_g of C_{6h} —can give rise to a SDE. As a result of the reduced symmetry, the two different AM order parameters associated with B_{1g} and B_{2g} in D_{6h} now both transform under B_g of C_{6h} and can, hence, mix. Intro-

ducing a 3×3 matrix R_φ describing rotations by φ along the third direction, this admixture can be parametrized as

$$\mathbf{N}_\mathbf{k} = R_\varphi \mathbf{N}_\mathbf{k}^{B_{1g}} \sim N_0 R_\varphi (k_x^2 - k_y^2, -2k_x k_y, 0)^T, \quad (15)$$

where $\mathbf{N}_\mathbf{k}^{B_{1g}}$ is the B_{1g} AM order parameter of D_{6h} used above in Sec. III B and the asymptotic relation again refers to the vicinity of the Γ point, $\mathbf{k} \rightarrow 0$.

To obtain a finite SDE, $\eta \neq 0$, inversion symmetry I still needs to be broken by application of an electric field $E_z \neq 0$. This induces a spin-orbit coupling term $\mathbf{g}_\mathbf{k}$. For the same reason as above, the spin-orbit vector is less constrained than in D_{6h} and can be written in the form $R_\varphi \mathbf{g}_\mathbf{k}$, where $\mathbf{g}_\mathbf{k}$ is identical to the one used for D_{6h} above, obeying $\mathbf{g}_\mathbf{k} \sim \alpha(k_y, -k_x, 0)^T$. For $\mathbf{N}_\mathbf{k}$, $\mathbf{g}_\mathbf{k} \neq 0$, the residual magnetic point group of the system is generated by C_{3z} and $C_{2z}\Theta$. As such, the only constraints on the particle-particle bubble and the critical current are $\Gamma(\mathbf{q}) = \Gamma(C_{3z}\mathbf{q})$ and $J_c(\hat{\mathbf{n}}) = J_c(C_{3z}\hat{\mathbf{n}})$, which are clearly visible in our numerical results in Fig. 3(a) and (b), respectively. As expected, the maxima and minima of these two quantities are not pinned along high-symmetry directions and, therefore, the zeros of $\eta(\hat{\mathbf{n}})$, shown in Fig. 3(c), are not pinned either.

We further present in Fig. 3(d) the diode efficiency η for both the magnetic field-induced SDE and the altermagnetic SDE. To treat them on equal footing, we use the same model and set $\mathbf{B}^2 = N_0^2 = \sum_{\mathbf{k} \in \text{BZ}} \mathbf{N}_\mathbf{k}^2$. Employing the same parameters as in the other parts of Fig. 3, we find that the efficiency is significantly larger in the AM case; this demonstrates that the AM SDE is *not* a subleading and, thus generally, weaker effect compared to the magnetic-field-induced one, contrary to what one might have expected since the average magnetization is required to vanish for an AM. However, we caution that both magnetic fields and AMs can yield sizeable SDE with relative magnitudes depending largely on the parameters chosen.

D. E_z tunable zeros and polarization in D_3

We finally discuss the AM-induced SDE for the case where \mathcal{G}_0 is already a non-centrosymmetric point group. As such, an electric field will not be required to get a SDE. Nonetheless, as we will see, E_z can still be used to tune the properties of the system in a non-trivial way. For concreteness, let us choose $\mathcal{G}_0 = D_3$. As can be seen in Table I, there is only a single AM order parameter, transforming under the trivial representation of the point group. While, to leading (quadratic) order in \mathbf{k} , it has the same form as $\mathbf{N}_\mathbf{k}$ in Eq. (13), the subleading corrections are different. In particular, the reduced symmetries allow

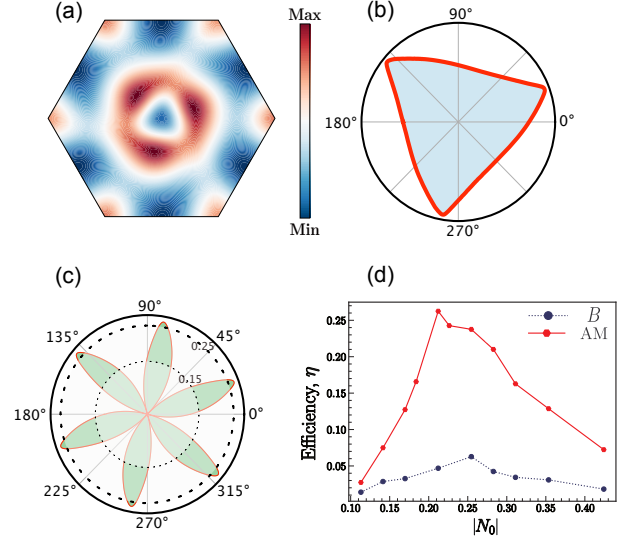


FIG. 3: SDE in the point group C_{6h} at $E_z \neq 0$. (a) Particle-particle bubble $\Gamma(\mathbf{q})$ in the Brillouin zone; (b) shows the critical current $J_c(\hat{\mathbf{n}})$ as a function of direction $\hat{\mathbf{n}}$ for $N_0 = -0.21$; (c) displays the angle-resolved SDE efficiency $\eta(\hat{\mathbf{n}})$. Due to the reduced symmetry compared to D_{6h} [cf. Fig. 2b(iv)], the zeros (and also maxima) of η are rotated away from high-symmetry directions; (d) SDE efficiency η as a function of magnetic field and altermagnetic order parameter N_0 shown in blue and red respectively. The magnetic field is chosen along the x direction. In this figure, we used $\alpha = 0.4$, $t' = 0.05t$, $g^{-1} = 0.5\Gamma(\mathbf{q} = 0)$, $\varphi = -0.25\pi$, $\varphi' = 0$.

for a finite $(\mathbf{N}_\mathbf{k})_z$ component;

$$\mathbf{N}_\mathbf{k} \sim N_0 (k_x^2 - k_y^2, -2k_x k_y, \tau k_x k_y (k_x^2 - 3k_y^2) (k_y^2 - 3k_x^2)), \quad (16)$$

where we only kept the leading term in every component and τ is a real parameter that is not determined by symmetry. The total spin polarization still vanishes, $\langle \mathbf{S} \rangle = 0$, as required for an AM, which follows from the preserved C_{3z} ($\langle S_{x,y} \rangle = 0$) and C_{2x} ($\langle S_z \rangle = 0$) symmetries.

Interestingly, the spin-orbit vector has two different contributions, $\mathbf{g}_\mathbf{k} = \mathbf{g}_\mathbf{k}^I + \mathbf{g}_\mathbf{k}^{II}$ where $\mathbf{g}_\mathbf{k}^I \sim \beta(k_x, k_y, k_y(3k_x^2 - k_y^2))$ is already allowed by the point group D_3 without the need of an external electric field, and $\mathbf{g}_\mathbf{k}^{II} \sim \alpha(k_y, -k_x, k_x(k_x^2 - 3k_y^2))$ is the spin-orbit coupling term induced by a perpendicular electric field E_z , i.e., $\alpha \propto E_z + \mathcal{O}(E_z^3)$. The full expressions for $\mathbf{N}_\mathbf{k}$, $\mathbf{g}_\mathbf{k}^I$, and $\mathbf{g}_\mathbf{k}^{II}$ we use are provided in Appendix B. Finally, for the dispersion, we restrict ourselves just to a nearest-neighbor hopping term on the triangular lattice, $\epsilon_\mathbf{k} = -\sum_{j=1}^3 t \cos(\mathbf{a}_j \cdot \mathbf{k})$.

Let us first focus on $E_z = 0$ ($\alpha = 0$). Since C_{2z} , I , and Θ are already broken, we find a finite SDE, see Fig. 4(a,b). Furthermore, we observe that the extrema of the critical current rotated by 90° in comparison to D_{6h} [cf. Fig. 2(biii)]. This is closely related to the discussion

in Sec. II A; since D_3 has two-fold rotational symmetry C_{2x} about the in-plane direction x , the current has to obey $J_c(C_{2x}\hat{n}) = J_c(\hat{n})$ which pins its extrema along \hat{e}_x and C_{3z} -related directions. Similarly, Eq. (3) implies that the angle-resolved efficiency $\eta(\hat{n})$ has to go to zero for $\hat{n} = \hat{e}_y$, $C_{3z}\hat{e}_y$ and $C_{3z}^2\hat{e}_y$, which is also observed in our numerics [see Fig. 4(b)].

To demonstrate the effect of a finite E_z , we repeat the analysis now in the presence of the induced spin-orbit coupling term $g_{\mathbf{k}}^{\text{II}}$. The electric field transforms as A_2 of D_3 and reduces the point group to C_3 . Altogether, since time-reversal and inversion are still broken, the system still shows a SDE, see Fig. 4(c,d), only now that there is no two-fold in-plane rotation (C_{2x}) or a mirror-plane $\sigma_{\hat{m}}$ as a symmetry. Naturally, it follows that the zeros of $\eta(\hat{n})$ are not pinned to the high symmetry directions, but are now free to move in-plane, as is clearly visible in Fig. 4(d). An electric field can thus be used to tune the orientation of the zeros of the SDE efficiency $\eta(\hat{n})$.

By the same token, we also find that the E_z -induced reduction of the point group leads to the order parameter lose its AM nature—since all in-plane rotations are broken, we expect $\langle S_z \rangle \neq 0$ for $\alpha \neq 0$; meanwhile we still have $\langle S_{x,y} \rangle = 0$ since C_{3z} remains unbroken. This is indeed what we find when computing the expectation value of the spin operators in Eq. (7) explicitly within our model, with the result displayed in Fig. 4(e). We can further see that the orientation of the spin polarization can be swapped by changing the sign of α , as expected by symmetry, and also by increasing $|\alpha|$ beyond a certain magnitude. To understand the latter observation better, we consider the inset in Fig. 4(e), which shows the contributions from the bands $\sigma = \pm 1$ to the total polarization. As we start increasing α in the positive direction, for very small values of α , the $\sigma = -1$ band (shown in green) starts contributing more than its counterpart $\sigma = 1$ (shown in orange) to $\langle S_z \rangle$. This happens until a certain value of α is reached from whence the $\sigma = 1$ starts taking over and ends up contributing the bulk of the total polarization, thereby flipping the value of $\langle S_z \rangle$. This flipping of polarization on the same side can also be well understood by noting that at $\alpha = 0.05t$, both Fermi surfaces [see Fig. 4(f)] corresponding to $\sigma = \pm 1$, shown in orange and green respectively contribute. Meanwhile, when $\alpha = 0.1t$, only the green one contributes to the spin polarization. Taken together, we see that an AM order parameter in the non-centrosymmetric point group D_3 (same applies to D_6 , see Table I) can induce a SDE, with both the zeros in the efficiency $\eta(\hat{n})$ and the spin polarization being tunable by an applied electric field E_z .

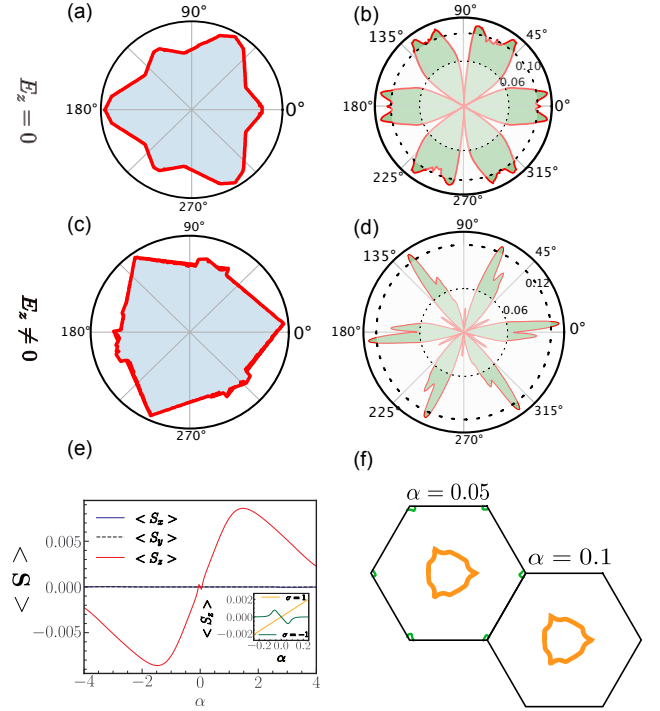


FIG. 4: SDE in the non-centrosymmetric point group D_3 . (a) and (c) show the directional-dependence of the critical current $J_c(\hat{n})$ for zero and finite electric field, respectively. The corresponding SDE efficiencies $\eta(\hat{n})$ are displayed in (b) and (d). Since $E_z \neq 0$ breaks all in-plane rotation symmetries $C_{2\hat{m}}$, it can be used to rotate the symmetry-imposed zeros of $\eta(\hat{n})$ away from high-symmetry directions. It can also be used, to control the net magnetization, see (e), where the spin polarization as a function of E_z is shown; the inset is a zoomed-in version of the respective contribution of the two bands (in orange and green) to $\langle S_z \rangle$. (f) reveals that both Fermi surfaces (corresponding to the two bands) are present for $\alpha = 0.05$ and, for $\alpha = 0.1$, only one of the bands contribute. Explicit parameters are given in [120].

IV. CONCLUSION

In this work, we have studied under which conditions a conventional two-dimensional superconducting phase can exhibit a SDE, $\eta_s \neq 0$ in Eq. (2), if the only source of broken time-reversal symmetry is an AM order parameter. To approach this question systematically, we started by listing all AM order parameters $N_{\mathbf{k}}$, coupling to the electrons as given by Eq. (5), for all possible 2D crystalline point groups, see Table I. For each of them, we checked whether there are still residual symmetries, such as inversion symmetry or two-fold rotation along a direction perpendicular to the plane of the system, that would enforce the critical currents along opposite directions to be the same, $J_c(\hat{n}) = J_c(-\hat{n})$. We found that there are indeed several point groups and associated AM

order parameters (C_{6h} with AM in B_g ; D_{6h} with AM in B_{1g} and B_{2g} ; D_{3d} with A_{1g} ; D_3 with AM in A_1 ; D_6 with B_1 and B_2) that give rise to an SDE, as we have also checked by explicit model calculations. Since, by design, the total magnetic moment vanishes when an AM is the only source of broken time-reversal symmetry, this demonstrates that the SDE does not require finite net magnetization. A direct comparison with the magnetic-field-induced SDE reveals that the altermagnetic SDE is not a subleading effect; in fact, depending on parameters, the altermagnetic efficiency can even be substantially larger when compared in the same model with the magnetic-field scenario.

In the context of the SDE, the AM order parameters can be further categorized in the following way: the AMs transforming under B_g of C_{6h} , B_{1g} or B_{2g} of D_{6h} , and A_{1g} of D_{3d} will only give rise to an SDE if also an electric field, E_z , perpendicular to the plane of the system is applied. This breaks inversion symmetry, a necessary requirement for the SDE. Note, however, that in all cases listed here, there are still enough symmetries present to guarantee a vanishing net magnetic moment. This shows that AMs allow for electric-field-tunable (rather than the frequently discussed magnetic-field-tunable) SDEs. In turn, the AMs transforming under A_1 and $B_{1,2}$ for the non-centrosymmetric point groups D_3 and D_6 , respectively, will immediately give rise to a SDE, without application of an electric field; moreover, for $E_z \neq 0$, the symmetries will be lowered in such a way that the order parameters cease to be AMs. Here the electric field can be used to control the out-of-plane magnetization of the system.

Another important distinction of the different scenarios for AM-induced SDEs can be made based on the directions \hat{n}_j where the SDE efficiency vanishes, $\eta(\hat{n}_j) = 0$. While \hat{n}_j are pinned along high-symmetry directions for D_{6h} (reduced to C_{6v} by $E_z \neq 0$) and D_{3d} (reduced to

C_{3v}), this is not the case for the SDEs induced by the B_g AM in C_{6h} (reduced to C_6), where \hat{n}_j point along generic (C_{3z} -related) directions. Finally, for the AMs of non-centrosymmetric point groups D_3 and D_6 that can induce an SDE, applying an electric field $E_z \neq 0$ allows to rotate the \hat{n}_j with $\eta(\hat{n}_j) = 0$ away from crystalline to generic directions.

These findings, that can be deduced from symmetry considerations, are summarized in Table I. We have further constructed and solved minimal lattice models for the different classes of and phenomena associated with AM-induced SDEs discussed above. This further illustrates and explicitly demonstrates the complex interplay of AM and superconductivity. We finally point out that there are several setups that can be used to realize and probe the proposed AM-induced SDE experimentally, see Fig. 1. Given that there are already candidate materials with the right symmetries (see last column in Table I), the rapidly growing number of AM candidate materials [26], and the fact that heterostructures are routinely grown or stacked, this seems to be well within current experimental reach.

ACKNOWLEDGMENTS

S.B. and M.S.S. acknowledge funding by the European Union (ERC-2021-STG, Project 101040651—SuperCorr). Views and opinions expressed are however those of the authors only and do not necessarily reflect those of the European Union or the European Research Council Executive Agency. Neither the European Union nor the granting authority can be held responsible for them. The data sets generated in this study are available in the Zenodo database under the accession code <https://zenodo.org/records/12794241>. The authors thank P. McClarty, R. Fernandes, L. Pupim, A. Rastogi and J. Sobral for discussions.

-
- [1] L.-D. Yuan, Z. Wang, J.-W. Luo, E. I. Rashba, and A. Zunger, “Giant momentum-dependent spin splitting in centrosymmetric low- Z antiferromagnets,” *Physical Review B* **102**, 014422 (2020).
 - [2] L. Šmejkal, J. Sinova, and T. Jungwirth, “Beyond Conventional Ferromagnetism and Antiferromagnetism: A Phase with Nonrelativistic Spin and Crystal Rotation Symmetry,” *Physical Review X* **12**, 031042 (2022).
 - [3] L. Šmejkal, J. Sinova, and T. Jungwirth, “Emerging Research Landscape of Altermagnetism,” *Physical Review X* **12**, 040501 (2022).
 - [4] K.-H. Ahn, A. Hariki, K.-W. Lee, and J. Kuneš, “Antiferromagnetism in RuO₂ as d-wave Pomeranchuk instability,” *Physical Review B* **99**, 184432 (2019).
 - [5] S. Bhowal and N. A. Spaldin, “Magnetic octupoles as

- the order parameter for unconventional antiferromagnetism,” (2022), [arxiv:2212.03756](https://arxiv.org/abs/2212.03756) [cond-mat].
- [6] G. Cuono, R. M. Sattigeri, J. Skolimowski, and C. Autieri, “Orbital-selective altermagnetism and correlation-enhanced spin-splitting in transition metal oxides,” *Journal of Magnetism and Magnetic Materials* **586**, 171163 (2023), [arxiv:2306.17497](https://arxiv.org/abs/2306.17497) [cond-mat].
- [7] Y. Guo, H. Liu, O. Janson, I. C. Fulga, J. van den Brink, and J. I. Facio, “Spin-split collinear antiferromagnets: A large-scale ab-initio study,” *Materials Today Physics* **32**, 100991 (2023), [arxiv:2207.07592](https://arxiv.org/abs/2207.07592) [cond-mat].
- [8] T. A. Maier and S. Okamoto, “Weak-coupling theory of neutron scattering as a probe of altermagnetism,” *Physical Review B* **108**, L100402 (2023).
- [9] I. I. Mazin, “Altermagnetism in MnTe: Origin, pre-

- dicted manifestations, and routes to detwinning,” *Physical Review B* **107**, L100418 (2023).
- [10] V. Oganessian, S. A. Kivelson, and E. Fradkin, “Quantum theory of a nematic Fermi fluid,” *Physical Review B* **64**, 195109 (2001).
- [11] T. Sato, S. Haddad, I. C. Fulga, F. F. Assaad, and J. van den Brink, “Altermagnetic anomalous Hall effect emerging from electronic correlations,” (2023), [arxiv:2312.16290 \[cond-mat\]](#).
- [12] C. R. W. Steward, R. M. Fernandes, and J. Schmalian, “Dynamic paramagnon-polarons in altermagnets,” *Physical Review B* **108**, 144418 (2023).
- [13] I. Turek, “Altermagnetism and magnetic groups with pseudoscalar electron spin,” *Physical Review B* **106**, 094432 (2022).
- [14] J. A. Ouassou, A. Brataas, and J. Linder, “Dc Josephson Effect in Altermagnets,” *Physical Review Letters* **131**, 076003 (2023).
- [15] I. I. Mazin, K. Koepernik, M. D. Johannes, R. González-Hernández, and L. Šmejkal, “Prediction of unconventional magnetism in doped FeSb₂,” *Proceedings of the National Academy of Sciences* **118**, e2108924118 (2021).
- [16] S. Hayami, Y. Yanagi, and H. Kusunose, “Momentum-dependent spin splitting by collinear antiferromagnetic ordering,” *Journal of the Physical Society of Japan* **88**, 123702 (2019).
- [17] L. Šmejkal, R. González-Hernández, T. Jungwirth, and J. Sinova, “Crystal time-reversal symmetry breaking and spontaneous hall effect in collinear antiferromagnets,” *Science Advances* **6**, eaaz8809 (2020).
- [18] B. Brekke, A. Brataas, and A. Sudbø, “Two-dimensional altermagnets: Superconductivity in a minimal microscopic model,” *Physical Review B* **108**, 224421 (2023).
- [19] P. Das, V. Leeb, J. Knolle, and M. Knap, “Realizing Altermagnetism in Fermi-Hubbard Models with Ultracold Atoms,” (2023), [arxiv:2312.10151 \[cond-mat, physics:quant-ph\]](#).
- [20] A. Fakhredine, R. M. Sattigeri, G. Cuono, and C. Autieri, “Interplay between altermagnetism and nonsym-morphic symmetries generating large anomalous Hall conductivity by semi-Dirac points induced anticrossings,” *Physical Review B* **108**, 115138 (2023).
- [21] Y. Fang, J. Cano, and S. A. A. Ghorashi, “Quantum geometry induced nonlinear transport in altermagnets,” (2023), [arxiv:2310.11489 \[cond-mat\]](#).
- [22] V. Leeb, A. Mook, L. Šmejkal, and J. Knolle, “Spontaneous Formation of Altermagnetism from Orbital Ordering,” (2023), [arxiv:2312.10839 \[cond-mat\]](#).
- [23] I. Mazin, R. González-Hernández, and L. Šmejkal, “Induced Monolayer Altermagnetism in MnP(S,Se)₃ and FeSe,” (2023), [arxiv:2309.02355 \[cond-mat\]](#).
- [24] L. Šmejkal, A. Marmodoro, K.-H. Ahn, R. González-Hernández, I. Turek, S. Mankovsky, H. Ebert, S. W. D’Souza, O. Šipr, J. Sinova, and T. Jungwirth, “Chiral Magnons in Altermagnetic RuO₂,” *Physical Review Letters* **131**, 256703 (2023).
- [25] C. Sun and J. Linder, “Spin pumping from a ferromagnetic insulator into an altermagnet,” *Physical Review B* **108**, L140408 (2023).
- [26] Z.-F. Gao, S. Qu, B. Zeng, Y. Liu, J.-R. Wen, H. Sun, P.-J. Guo, and Z.-Y. Lu, “AI-accelerated Discovery of Altermagnetic Materials,” (2023), [arxiv:2311.04418 \[cond-mat, physics:physics\]](#).
- [27] C. W. J. Beenakker and T. Vakh-tel, “Phase-shifted Andreev levels in an altermagnet Josephson junction,” *Physical Review B* **108**, 075425 (2023).
- [28] X. Zhou, W. Feng, R.-W. Zhang, L. Šmejkal, J. Sinova, Y. Mokrousov, and Y. Yao, “Crystal thermal transport in altermagnetic RuO₂,” *Phys. Rev. Lett.* **132**, 056701 (2024).
- [29] R. M. Fernandes, V. S. de Carvalho, T. Birol, and R. G. Pereira, “Topological transition from nodal to nodeless Zeeman splitting in altermagnets,” *arXiv e-prints* (2023), [arXiv:2307.12380 \[cond-mat.mes-hall\]](#).
- [30] C. Sun, A. Brataas, and J. Linder, “Andreev reflection in altermagnets,” *Phys. Rev. B* **108**, 054511 (2023).
- [31] S.-B. Zhang, L.-H. Hu, and T. Neupert, “Finite-momentum cooper pairing in proximitized altermagnets,” (2023), [arXiv:2302.13185 \[cond-mat.supr-con\]](#).
- [32] H. G. Giil and J. Linder, “Superconductor-altermagnet memory functionality without stray fields,” (2023), [arXiv:2308.10939 \[cond-mat.supr-con\]](#).
- [33] D. Zhu, Z.-Y. Zhuang, Z. Wu, and Z. Yan, “Topological superconductivity in two-dimensional altermagnetic metals,” *Phys. Rev. B* **108**, 184505 (2023).
- [34] Y.-X. Li and C.-C. Liu, “Majorana corner modes and tunable patterns in an altermagnet heterostructure,” *Phys. Rev. B* **108**, 205410 (2023).
- [35] S. A. A. Ghorashi, T. L. Hughes, and J. Cano, “Altermagnetic routes to majorana modes in zero net magnetization,” (2023), [arXiv:2306.09413 \[cond-mat.mes-hall\]](#).
- [36] Q. Cheng and Q.-F. Sun, “Orientation-dependent josephson effect in spin-singlet superconductor/altermagnet/spin-triplet superconductor junctions,” *Phys. Rev. B* **109**, 024517 (2024).
- [37] D. S. Antonenko, R. M. Fernandes, and J. W. F. Venderbos, “Mirror chern bands and weyl nodal loops in altermagnets,” (2024), [arXiv:2402.10201 \[cond-mat.mes-hall\]](#).
- [38] Y. Yu, H.-G. Suh, M. Roig, and D. F. Agterberg, “Altermagnetism from coincident van hove singularities: application to κ -cl,” (2024), [arXiv:2402.05180 \[cond-mat.str-el\]](#).
- [39] M. Wei, L. Xiang, F. Xu, L. Zhang, G. Tang, and J. Wang, “Gapless superconducting state and mirage gap in altermagnets,” (2023), [arXiv:2308.00248 \[cond-mat.supr-con\]](#).
- [40] P. A. McClarty and J. G. Rau, “Landau theory of altermagnetism,” (2023), [arXiv:2308.04484 \[cond-mat.mtrl-sci\]](#).
- [41] T. Aoyama and K. Ohgushi, “Piezomagnetic Properties in Altermagnetic MnTe,” (2023), [arxiv:2305.14786 \[cond-mat\]](#).
- [42] H. Bai, Y. C. Zhang, Y. J. Zhou, P. Chen, C. H. Wan, L. Han, W. X. Zhu, S. X. Liang, Y. C. Su, X. F. Han, F. Pan, and C. Song, “Efficient Spin-to-Charge Conversion via Altermagnetic Spin Splitting Effect in Antiferromagnet RuO₂,” *Physical Review Letters* **130**, 216701 (2023).
- [43] J. Krempaský, L. Šmejkal, S. W. D’Souza, M. Hajlaoui, G. Springholz, K. Uhlířová, F. Alarab, P. C.

- Constantinou, V. Strokov, D. Usanov, W. R. Pudenko, R. González-Hernández, A. B. Hellenes, Z. Jansa, H. Reichlová, Z. Šobán, R. D. G. Betancourt, P. Wadley, J. Sinova, D. Kriegner, J. Minár, J. H. Dil, and T. Jungwirth, “Altermagnetic lifting of Kramers spin degeneracy,” (2023), [arxiv:2308.10681 \[cond-mat, physics:physics\]](#).
- [44] S. Lee, S. Lee, S. Jung, J. Jung, D. Kim, Y. Lee, B. Seok, J. Kim, B. G. Park, L. Šmejkal, C.-J. Kang, and C. Kim, “Broken Kramers’ degeneracy in altermagnetic MnTe,” (2023), [arxiv:2308.11180 \[cond-mat\]](#).
- [45] S. Reimers, L. Odenbreit, L. Šmejkal, V. N. Strocov, P. Constantinou, A. B. Hellenes, R. J. Ubierto, W. H. Campos, V. K. Bharadwaj, A. Chakraborty, T. Denneulin, W. Shi, R. E. Dunin-Borkowski, S. Das, M. Kläui, J. Sinova, and M. Jourdan, “Direct observation of altermagnetic band splitting in CrSb thin films,” (2023), [arxiv:2310.17280 \[cond-mat\]](#).
- [46] Z. Feng, X. Zhou, L. Šmejkal, L. Wu, Z. Zhu, H. Guo, R. González-Hernández, X. Wang, H. Yan, P. Qin, X. Zhang, H. Wu, H. Chen, Z. Meng, L. Liu, Z. Xia, J. Sinova, T. Jungwirth, and Z. Liu, “An anomalous Hall effect in altermagnetic ruthenium dioxide,” *Nature Electronics* **5**, 735 (2022).
- [47] A. Bose, N. J. Schreiber, R. Jain, D.-F. Shao, H. P. Nair, J. Sun, X. S. Zhang, D. A. Muller, E. Y. Tsymlal, D. G. Schlom, and D. C. Ralph, “Tilted spin current generated by the collinear antiferromagnet ruthenium dioxide,” *Nature Electronics* **5**, 267 (2022).
- [48] P. I., “On the stability of a fermi liquid,” *Sov. Phys. JETP* **8**, 361 (1958).
- [49] C. Wu, K. Sun, E. Fradkin, and S.-C. Zhang, “Fermi liquid instabilities in the spin channel,” *Physical Review B* **75**, 115103 (2007).
- [50] B. Chi, L. Jiang, Y. Zhu, G. Yu, C. Wan, J. Zhang, and X. Han, “Crystal facet orientated altermagnets for detecting ferromagnetic and antiferromagnetic states by giant tunneling magnetoresistance effect,” (2023), [arXiv:2309.09561 \[cond-mat.mtrl-sci\]](#).
- [51] D. Chakraborty and A. M. Black-Schaffer, “Zero-field finite-momentum and field-induced superconductivity in altermagnets,” (2023), [arxiv:2309.14427 \[cond-mat\]](#).
- [52] X. Jiang, P. J. Connolly, S. J. Hagen, and C. J. Lobb, “Asymmetric current-voltage characteristics in type-II superconductors,” *Phys. Rev. B* **49**, 9244 (1994).
- [53] F. Ando, Y. Miyasaka, T. Li, J. Ishizuka, T. Arakawa, Y. Shiota, T. Moriyama, Y. Yanase, and T. Ono, “Observation of superconducting diode effect,” *Nature* **584**, 373 (2020).
- [54] Y.-Y. Lyu, J. Jiang, Y.-L. Wang, Z.-L. Xiao, S. Dong, Q.-H. Chen, M. V. Milošević, H. Wang, R. Divan, J. E. Pearson, P. Wu, F. M. Peeters, and W.-K. Kwok, “Superconducting diode effect via conformal-mapped nanoholes,” *Nature Communications* **12**, 1 (2021).
- [55] W.-S. Du, W. Chen, Y. Zhou, T. Zhou, G. Liu, Z. Zhang, Z. Miao, H. Jia, S. Liu, Y. Zhao, Z. Zhang, T. Chen, N. Wang, W. Huang, Z.-B. Tan, J.-J. Chen, and D.-P. Yu, “Superconducting Diode Effect and Large Magnetochiral Anisotropy in T_d-MoTe₂ Thin Film,” (2023), [arxiv:arXiv:2303.09052](#).
- [56] A. Sundares, J. I. Vayrynen, Y. Lyanda-Geller, and L. P. Rokhinson, “Diamagnetic mechanism of critical current non-reciprocity in multilayered superconductors,” (2023), [arxiv:arXiv:2207.03633](#).
- [57] R. Kealhofer, H. Jeong, A. Rashidi, L. Balents, and S. Stemmer, “Anomalous superconducting diode effect in a polar superconductor,” *Physical Review B* **107**, L100504 (2023), [arxiv:2303.16238 \[cond-mat\]](#).
- [58] Y. Hou, F. Nichele, H. Chi, A. Lodesani, Y. Wu, M. F. Ritter, D. Z. Haxell, M. Davydova, S. Ilić, O. Glezakou-Elbert, A. Varambally, F. S. Bergeret, A. Kamra, L. Fu, P. A. Lee, and J. S. Moodera, “Ubiquitous Superconducting Diode Effect in Superconductor Thin Films,” (2023), [arxiv:arXiv:2205.09276](#).
- [59] P. B. Chen, B. C. Ye, J. H. Wang, L. Zhou, X. Lei, Z. Z. Tang, J. N. Wang, J. W. Mei, and H. T. He, “Superconducting diode effect in inversion symmetry breaking MoTe₂ Josephson junctions,” (2023), [arxiv:arXiv:2303.07701](#).
- [60] M. Gupta, G. V. Graziano, M. Pendharkar, J. T. Dong, C. P. Dempsey, C. Palmström, and V. S. Pribiag, “Superconducting Diode Effect in a Three-terminal Josephson Device,” (2022), [arxiv:arXiv:2206.08471](#).
- [61] C. Baumgartner, L. Fuchs, A. Costa, S. Reinhardt, S. Gronin, G. C. Gardner, T. Lindemann, M. J. Manfra, P. E. Faria Junior, D. Kochan, J. Fabian, N. Paradiso, and C. Strunk, “Supercurrent rectification and magnetochiral effects in symmetric josephson junctions,” *Nature Nanotechnology* **17**, 39 (2022).
- [62] A. Banerjee, M. Geier, M. A. Rahman, C. Thomas, T. Wang, M. J. Manfra, K. Flensberg, and C. M. Marcus, “Phase Asymmetry of Andreev Spectra From Cooper-Pair Momentum,” (2023), [arxiv:arXiv:2301.01881](#).
- [63] B. Pal, A. Chakraborty, P. K. Sivakumar, M. Davydova, A. K. Gopi, A. K. Pandeya, J. A. Krieger, Y. Zhang, M. Date, S. Ju, N. Yuan, N. B. M. Schröter, L. Fu, and S. S. P. Parkin, “Josephson diode effect from Cooper pair momentum in a topological semimetal,” *Nature Physics* **1** (2022).
- [64] J.-K. Kim, K.-R. Jeon, P. K. Sivakumar, J. Jeon, C. Koenner, G. Woltersdorf, and S. S. P. Parkin, “Intrinsic supercurrent non-reciprocity coupled to the crystal structure of a van der Waals Josephson barrier,” (2023), [arxiv:arXiv:2303.13049](#).
- [65] B. Turini, S. Salimian, M. Carrega, A. Iorio, E. Strambini, F. Giazotto, V. Zannier, L. Sorba, and S. Heun, “Josephson diode effect in high-mobility insb nanoflags,” *Nano Letters* **22**, 8502 (2022).
- [66] L. Bauriedl, C. Bäuml, L. Fuchs, C. Baumgartner, N. Paulik, J. M. Bauer, K.-Q. Lin, J. M. Lupton, T. Taniguchi, K. Watanabe, C. Strunk, and N. Paradiso, “Supercurrent diode effect and magnetochiral anisotropy in few-layer nbse₂,” *Nature Communications* **13**, 4266 (2022).
- [67] H. Wu, Y. Wang, Y. Xu, P. K. Sivakumar, C. Pasco, U. Filippozzi, S. S. P. Parkin, Y.-J. Zeng, T. McQueen, and M. N. Ali, “The field-free Josephson diode in a van der Waals heterostructure,” *Nature* **604**, 653 (2022).
- [68] J. Diez-Merida, A. Diez-Carlon, S. Y. Yang, Y.-M. Xie, X.-J. Gao, K. Watanabe, T. Taniguchi, X. Lu, K. T. Law, and D. K. Efetov, “Magnetic Josephson Junctions

- and Superconducting Diodes in Magic Angle Twisted Bilayer Graphene,” (2021), [arXiv:arXiv:2110.01067](#).
- [69] T. Golod and V. M. Krasnov, “Demonstration of a superconducting diode-with-memory, operational at zero magnetic field with switchable nonreciprocity,” *Nature Communications* **13**, 3658 (2022).
- [70] J. Chiles, E. G. Arnault, C.-C. Chen, T. F. Q. Larson, L. Zhao, K. Watanabe, T. Taniguchi, F. Amet, and G. Finkelstein, “Non-Reciprocal Supercurrents in a Field-Free Graphene Josephson Triode,” (2022), [arXiv:arXiv:2210.02644](#).
- [71] F. Zhang, M. T. Ahari, A. S. Rashid, G. J. de Coster, T. Taniguchi, K. Watanabe, M. J. Gilbert, N. Samarth, and M. Kayyalha, “Reconfigurable magnetic-field-free superconducting diode effect in multi-terminal Josephson junctions,” (2023), [arXiv:arXiv:2301.05081](#).
- [72] J. Shin, S. Son, J. Yun, G. Park, K. Zhang, Y. J. Shin, J.-G. Park, and D. Kim, “Magnetic Proximity-Induced Superconducting Diode Effect and Infinite Magnetoresistance in van der Waals Heterostructure,” (2021), [arXiv:arXiv:2111.05627](#).
- [73] K.-R. Jeon, J.-K. Kim, J. Yoon, J.-C. Jeon, H. Han, A. Cottet, T. Kontos, and S. S. P. Parkin, “Zero-field polarity-reversible Josephson supercurrent diodes enabled by a proximity-magnetized Pt barrier,” *Nature Materials* **21**, 1008 (2022).
- [74] J.-X. Lin, P. Siriviboon, H. D. Scammell, S. Liu, D. Rhodes, K. Watanabe, T. Taniguchi, J. Hone, M. S. Scheurer, and J. I. A. Li, “Zero-field superconducting diode effect in small-twist-angle trilayer graphene,” *Nature Physics* **18**, 1221 (2022).
- [75] M. S. Anwar, T. Nakamura, R. Ishiguro, S. Arif, J. W. A. Robinson, S. Yonezawa, M. Sigrist, and Y. Maeno, “Spontaneous superconducting diode effect in non-magnetic Nb/Ru/Sr₂RuO₄ topological junctions,” (2022), [arXiv:arXiv:2211.14626](#).
- [76] H. Narita, J. Ishizuka, R. Kawarazaki, D. Kan, Y. Shiotani, T. Moriyama, Y. Shimakawa, A. V. Ognev, A. S. Samardak, Y. Yanase, and T. Ono, “Field-free superconducting diode effect in noncentrosymmetric superconductor/ferromagnet multilayers,” *Nature Nanotechnology* **17**, 823 (2022), [arXiv:2206.00483 \[cond-mat\]](#).
- [77] A. Gutfreund, H. Matsuki, V. Plastovets, A. Noah, L. Gorzawski, N. Fridman, G. Yang, A. Buzdin, O. Millo, J. W. A. Robinson, and Y. Anahory, “Direct Observation of a Superconducting Vortex Diode,” (2023), [arXiv:arXiv:2301.07121](#).
- [78] S. Y. F. Zhao, X. Cui, P. A. Volkov, H. Yoo, S. Lee, J. A. Gardener, A. J. Akey, R. Engelke, Y. Ronen, R. Zhong, G. Gu, S. Plugge, T. Tummuru, M. Kim, M. Franz, J. H. Pixley, N. Poccia, and P. Kim, “Time-reversal symmetry breaking superconductivity between twisted cuprate superconductors,” *Science* **382**, 1422 (2023), <https://www.science.org/doi/pdf/10.1126/science.abl8371>.
- [79] A. Daido and Y. Yanase, “Superconducting diode effect and nonreciprocal transition lines,” *Physical Review B* **106**, 205206 (2022).
- [80] A. Daido, Y. Ikeda, and Y. Yanase, “Intrinsic Superconducting Diode Effect,” *Physical Review Letters* **128**, 037001 (2022).
- [81] N. F. Q. Yuan and L. Fu, “Supercurrent diode effect and finite-momentum superconductors,” *Proceedings of the National Academy of Sciences* **119**, e2119548119 (2022).
- [82] J. J. He, Y. Tanaka, and N. Nagaosa, “A phenomenological theory of superconductor diodes,” *New Journal of Physics* **24**, 053014 (2022).
- [83] S. Ilić and F. S. Bergeret, “Theory of the Supercurrent Diode Effect in Rashba Superconductors with Arbitrary Disorder,” *Physical Review Letters* **128**, 177001 (2022).
- [84] H. D. Scammell, J. I. A. Li, and M. S. Scheurer, “Theory of zero-field superconducting diode effect in twisted trilayer graphene,” *2D Materials* **9**, 025027 (2022).
- [85] B. Zinkl, K. Hamamoto, and M. Sigrist, “Symmetry conditions for the superconducting diode effect in chiral superconductors,” *Physical Review Research* **4**, 033167 (2022).
- [86] Y. Zhang, Y. Gu, P. Li, J. Hu, and K. Jiang, “General theory of josephson diodes,” *Phys. Rev. X* **12**, 041013 (2022).
- [87] J. J. He, Y. Tanaka, and N. Nagaosa, “The supercurrent diode effect and nonreciprocal paraconductivity due to the chiral structure of nanotubes,” (2022), [arXiv:arXiv:2212.02183](#).
- [88] B. Zhai, B. Li, Y. Wen, F. Wu, and J. He, “Prediction of ferroelectric superconductors with reversible superconducting diode effect,” *Phys. Rev. B* **106**, L140505 (2022).
- [89] J. Jiang, M. Milošević, Y.-L. Wang, Z.-L. Xiao, F. Peeters, and Q.-H. Chen, “Field-Free Superconducting Diode in a Magnetically Nanostructured Superconductor,” *Physical Review Applied* **18**, 034064 (2022).
- [90] T. H. Kikkeler, A. A. Golubov, and F. S. Bergeret, “Field-free anomalous junction and superconducting diode effect in spin-split superconductor/topological insulator junctions,” *Physical Review B* **106**, 214504 (2022).
- [91] D. Debnath and P. Dutta, “Gate-tunable josephson diode effect in rashba spin-orbit coupled quantum dot junctions,” (2024), [arXiv:2402.00817 \[cond-mat.supr-con\]](#).
- [92] M. Chazono, S. Kanasugi, T. Kitamura, and Y. Yanase, “Piezoelectric effect and diode effect in anapole and monopole superconductors,” (2022), [arXiv:arXiv:2212.13102](#).
- [93] D. Y. Vodolazov and F. M. Peeters, “Superconducting rectifier based on the asymmetric surface barrier effect,” *Physical Review B* **72**, 172508 (2005).
- [94] T. de Picoli, Z. Blood, Y. Lyanda-Geller, and J. I. Väyrynen, “Superconducting diode effect in quasi-one-dimensional systems,” (2023), [arXiv:arXiv:2302.04277](#).
- [95] D. Kochan, A. Costa, I. Zhumagulov, and I. Žutić, “Phenomenological Theory of the Supercurrent Diode Effect: The Lifshitz Invariant,” (2023), [arXiv:arXiv:2303.11975](#).
- [96] Y. Ikeda, A. Daido, and Y. Yanase, “Intrinsic superconducting diode effect in disordered systems,” (2022), [arXiv:arXiv:2212.09211](#).
- [97] Y. Tanaka, B. Lu, and N. Nagaosa, “Theory of giant diode effect in d-wave superconductor junctions on the surface of a topological insulator,” *Physical Review B* **106**, 214524 (2022).
- [98] D. Wang, Q.-H. Wang, and C. Wu, “Symmetry Con-

- straints on Direct-Current Josephson Diodes,” (2022), [arxiv:arXiv:2209.12646](#).
- [99] R. Haenel and O. Can, “Superconducting diode from flux biased Josephson junction arrays,” (2022), [arxiv:arXiv:2212.02657](#).
- [100] H. F. Legg, K. Laubscher, D. Loss, and J. Klinovaja, “Parity protected superconducting diode effect in topological Josephson junctions,” (2023), [arxiv:arXiv:2301.13740](#).
- [101] J. J. Cuozzo, W. Pan, J. Shabani, and E. Rossi, “Microwave-Tunable Diode Effect in Asymmetric SQUIDs with Topological Josephson Junctions,” (2023), [arxiv:arXiv:2303.16931](#).
- [102] R. S. Souto, M. Leijnse, and C. Schrade, “Josephson Diode Effect in Supercurrent Interferometers,” *Physical Review Letters* **129**, 267702 (2022).
- [103] Q. Cheng and Q.-F. Sun, “Josephson diode based on conventional superconductors and a chiral quantum dot,” (2023), [arxiv:arXiv:2302.11144](#).
- [104] J. F. Steiner, L. Melischek, M. Trahms, K. J. Franke, and F. von Oppen, “Diode effects in current-biased Josephson junctions,” (2022), [arxiv:arXiv:2212.06866](#).
- [105] A. Costa, J. Fabian, and D. Kochan, “Microscopic study of the Josephson supercurrent diode effect in 2DEG-based Josephson junctions,” (2023), [arxiv:arXiv:2303.14823](#).
- [106] Y.-J. Wei, H.-L. Liu, J. Wang, and J.-F. Liu, “Supercurrent rectification effect in graphene-based Josephson junctions,” *Physical Review B* **106**, 165419 (2022).
- [107] H. F. Legg, D. Loss, and J. Klinovaja, “Superconducting diode effect due to magnetochiral anisotropy in topological insulators and Rashba nanowires,” *Physical Review B* **106**, 104501 (2022).
- [108] T. Karabassov, I. V. Bobkova, A. A. Golubov, and A. S. Vasenko, “Hybrid helical state and superconducting diode effect in superconductor/ferromagnet/topological insulator heterostructures,” *Physical Review B* **106**, 224509 (2022).
- [109] J.-X. Hu, Z.-T. Sun, Y.-M. Xie, and K. T. Law, “Josephson diode effect induced by valley polarization in twisted bilayer graphene,” *Phys. Rev. Lett.* **130**, 266003 (2023).
- [110] Y.-M. Wu, Z. Wu, and H. Yao, “Pair-density-wave and chiral superconductivity in twisted bilayer transition metal dichalcogenides,” *Phys. Rev. Lett.* **130**, 126001 (2023).
- [111] N. Nunchot and Y. Yanase, “Chiral superconducting diode effect by dzyaloshinsky-moriya interaction,” (2024), [arXiv:2402.00317 \[cond-mat.supr-con\]](#).
- [112] A. Daido and Y. Yanase, “Unidirectional superconductivity and diode effect induced by dissipation,” (2023), [arXiv:2310.02539 \[cond-mat.supr-con\]](#).
- [113] R. S. Souto, M. Leijnse, C. Schrade, M. Valentini, G. Katsaros, and J. Danon, “Tuning the josephson diode response with an ac current,” (2023), [arXiv:2312.09204 \[cond-mat.supr-con\]](#).
- [114] J. Cayao, N. Nagaosa, and Y. Tanaka, “Enhancing the josephson diode effect with majorana bound states,” *Phys. Rev. B* **109**, L081405 (2024).
- [115] S. Banerjee and M. S. Scheurer, “Enhanced superconducting diode effect due to coexisting phases,” *Phys. Rev. Lett.* **132**, 046003 (2024).
- [116] J.-H. Nie, T. Xie, G. Chen, W. Zhang, and Y.-S. Fu, “Moiré enhanced two-band superconductivity in a mnTe/nbSe2 heterojunction,” *Nano Letters* **23**, 8370 (2023), pMID: 37656911, <https://doi.org/10.1021/acs.nanolett.3c02772>.
- [117] R. D. Gonzalez Betancourt, J. Zubáč, R. Gonzalez-Hernandez, K. Geishendorf, Z. Šobán, G. Springholz, K. Olejník, L. Šmejkal, J. Sinova, T. Jungwirth, S. T. B. Goennenwein, A. Thomas, H. Reichlová, J. Železný, and D. Kriegner, “Spontaneous anomalous hall effect arising from an unconventional compensated magnetic phase in a semiconductor,” *Phys. Rev. Lett.* **130**, 036702 (2023).
- [118] T. Inoshita, M. Hirayama, N. Hamada, H. Hosono, and S. Murakami, “Topological semimetal phases manifested in transition metal dichalcogenides intercalated with 3d metals,” *Phys. Rev. B* **100**, 121112 (2019).
- [119] For a(i) weak altermagnetism $N_0 = -0.1, \alpha = 0$; a(ii) strong altermagnetism $N_0 = -0.2, \alpha = 0$; (b)(ii-iv) in presence of electric field E_z , $N_0 = -0.23, \alpha = 0.4$ and $g^{-1} = 0.5\Gamma(\mathbf{q} = 0)$. Note that α is proportional to both the intrinsic spin-orbit coupling and E_z .
- [120] For $E_z = 0$ we take $N_0 = -0.1, \beta = 0.7, \alpha = 0$ and $g^{-1} = 0.5\Gamma(\mathbf{q} = 0)$; for $E_z \neq 0$ in second row, $N_0 = -1.4, \tau = 1, \beta = 1.2, \alpha = 1.0$ and $g^{-1} = 0.8\Gamma(\mathbf{q} = 0)$; (e), (f) $N_0 = -1.4, \beta = 0.8$.

Appendix A: Expression for the particle-particle bubble

In this section, we state the expression for the particle-particle bubble in presence of both inter- and intraband pairings. Given the Hamiltonian, defined in Eq.(11), we begin by defining a few quantities,

$$l_{i,\mathbf{k},\mathbf{q}} = g_{i,\mathbf{k},\mathbf{q}} + N_{i,\mathbf{k},\mathbf{q}}, \quad i = x, y, z \quad g_{p,\mathbf{k},\mathbf{q}}^{\pm} = l_{x,\mathbf{k}+\mathbf{q}/2} \pm il_{y,\mathbf{k}+\mathbf{q}/2}, \quad g_{m,\mathbf{k},\mathbf{q}}^{\pm} = l_{x,-\mathbf{k}+\mathbf{q}/2} \pm il_{y,-\mathbf{k}+\mathbf{q}/2}. \quad (\text{A1})$$

In addition the renormalized energies are given as

$$\mathcal{E}_{\mathbf{k},\mathbf{q},p,\pm} = \epsilon_{\mathbf{k}+\mathbf{q}/2} \pm g_p, \quad \mathcal{E}_{\mathbf{k},\mathbf{q},m,\pm} = \epsilon_{-\mathbf{k}+\mathbf{q}/2} \pm g_m, \quad (\text{A2})$$

where $g_p^2 = \sum_{i=x,y,z} l_{i,\mathbf{k}+\mathbf{q}/2}^2$ and $g_m^2 = \sum_{i=x,y,z} l_{i,-\mathbf{k}+\mathbf{q}/2}^2$. Armed with these definitions, we can write down the various coherence factors $\Lambda_{\mathbf{k},\mathbf{q},\nu,\eta}$ for the spinful model as

$$\Lambda_{\mathbf{k},\mathbf{q},m,\mp} = \mp \frac{G_{\mathbf{k},\mathbf{q}}}{g_m(\mathcal{E}_{\mathbf{k},\mathbf{q},m,\mp} + \mathcal{E}_{\mathbf{k},\mathbf{q},p,+})(\mathcal{E}_{\mathbf{k},\mathbf{q},m,\mp} + \mathcal{E}_{\mathbf{k},\mathbf{q},p,-})} + \frac{2}{(\mathcal{E}_{\mathbf{k},\mathbf{q},m,\mp} + \mathcal{E}_{\mathbf{k},\mathbf{q},p,\mp})}; \quad (\text{A3})$$

$$\Lambda_{\mathbf{k},\mathbf{q},p,\mp} = \mp \frac{G_{\mathbf{k},\mathbf{q}}}{g_p(\mathcal{E}_{\mathbf{k},\mathbf{q},m,-} + \mathcal{E}_{\mathbf{k},\mathbf{q},p,\mp})(\mathcal{E}_{\mathbf{k},\mathbf{q},m,+} + \mathcal{E}_{\mathbf{k},\mathbf{q},p,\mp})} + \frac{2}{(\mathcal{E}_{\mathbf{k},\mathbf{q},m,\mp} + \mathcal{E}_{\mathbf{k},\mathbf{q},p,\mp})}; \quad (\text{A4})$$

where $G_{\mathbf{k},\mathbf{q}} = g_{m,\mathbf{k},\mathbf{q}}^+ g_{p,\mathbf{k},\mathbf{q}}^- + g_{m,\mathbf{k},\mathbf{q}}^- g_{p,\mathbf{k},\mathbf{q}}^+ + 2g_p g_m + 2l_{z,\mathbf{k}+\mathbf{q}/2} l_{z,-\mathbf{k}+\mathbf{q}/2}$. The final expression for the particle-particle bubble $\Gamma(\mathbf{q})$ then reads

$$\Gamma(\mathbf{q}) = \frac{1}{4} \sum_{\mathbf{k}} \left(\Lambda_{\mathbf{k},\mathbf{q},p,+} \tanh \frac{\mathcal{E}_{\mathbf{k},\mathbf{q},p,+}}{2T} + \Lambda_{\mathbf{k},\mathbf{q},p,-} \tanh \frac{\mathcal{E}_{\mathbf{k},\mathbf{q},p,-}}{2T} + \Lambda_{\mathbf{k},\mathbf{q},m,+} \tanh \frac{\mathcal{E}_{\mathbf{k},\mathbf{q},m,+}}{2T} + \Lambda_{\mathbf{k},\mathbf{q},m,-} \tanh \frac{\mathcal{E}_{\mathbf{k},\mathbf{q},m,-}}{2T} \right). \quad (\text{A5})$$

Appendix B: Details of the models

We here state the basis functions used to characterise the terms $\mathbf{N}_{\mathbf{k}}$ and $\mathbf{g}_{\mathbf{k}}$ of the Hamiltonian in Eq. (9) of the main text for various point groups. Applying the convention, where one of the primitive lattice vectors of the underlying triangular lattice is given by $\mathbf{a}_1 = (1,0)^T$, the leading basis functions explicitly read as

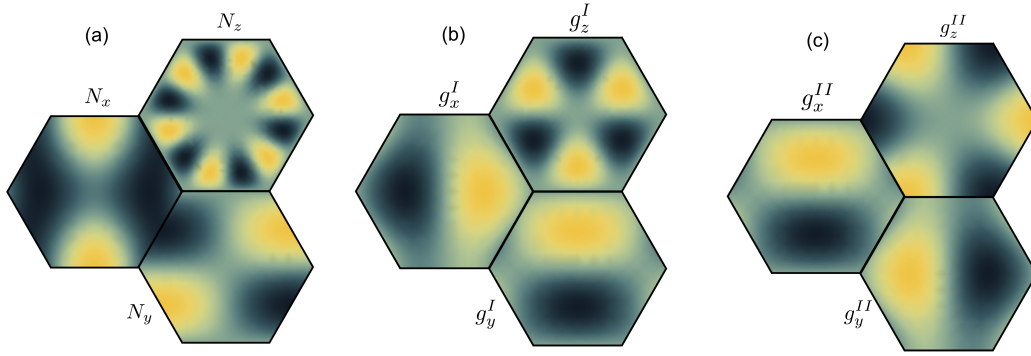


FIG. 5: Multi-component momentum dependence of (a) the altermagnet term $\mathbf{N}_{\mathbf{k}}$; (b) inversion-symmetry breaking term $\mathbf{g}_{\mathbf{k}}^I$ and (c) shows the spin-orbit coupling term $\mathbf{g}_{\mathbf{k}}^{II}$ induced by E_z . For point groups D_{6h} and C_{6h} , $\tau = 0$, $\tilde{\tau} = 0$ and $\beta = 0$, while for D_3 , $\tau \neq 0$, $\tilde{\tau} \neq 0$ and $\beta \neq 0$.

$$\mathbf{N}_{\mathbf{k}} = N_0 \left(\frac{-8}{3} (\cos k_x - \cos \frac{k_x}{2} \cos \frac{\sqrt{3}k_y}{2}), \frac{-8 \sin \frac{k_x}{2} \sin \frac{\sqrt{3}k_y}{2}}{\sqrt{3}}, 64\tau \frac{(\sin \frac{5k_x}{2} \sin \frac{3\sqrt{3}k_y}{2} + \sin \frac{k_x}{2} \sin \frac{\sqrt{3}k_y}{2} - \sin 2k_x \sin \sqrt{3}k_y)}{3\sqrt{3}} \right) \quad (\text{B1})$$

$$\mathbf{g}_{\mathbf{k}}^I = \beta \left(\frac{2}{3} (2 \cos \frac{k_x}{2} + \cos \frac{\sqrt{3}k_y}{2}) \sin \frac{k_x}{2}, \frac{2}{\sqrt{3}} \cos \frac{k_x}{2} \sin \frac{\sqrt{3}k_y}{2}, \frac{8(-2 \cos \frac{3k_x}{2} \sin \frac{\sqrt{3}k_y}{2} + \sin \sqrt{3}k_y)}{3\sqrt{3}} \right), \quad (\text{B2})$$

$$\mathbf{g}_{\mathbf{k}}^{II} = \alpha \left(\frac{2}{\sqrt{3}} \cos \frac{k_x}{2} \sin \frac{\sqrt{3}k_y}{2}, \frac{-2}{3} (2 \cos \frac{k_x}{2} + \cos \frac{\sqrt{3}k_y}{2}) \sin \frac{k_x}{2}, 16\tilde{\tau} \left(-\cos \frac{k_x}{2} + \cos \frac{\sqrt{3}k_y}{2} \right) \sin \frac{k_x}{2} \right). \quad (\text{B3})$$

These are the functions with the least number of nodes/nodal lines that satisfy the required symmetry constraints while being periodic on the Brillouin zone. As explained in the main text, $\tau = 0$ for point groups D_{6h} and C_{6h} and therefore Eq. (B1) reduces to Eq. (13) and Eq. (15), respectively, when expanded for small \mathbf{k} . As the point group D_3 permits the AM order parameter to also have a third component, it is given by Eq. (B1) with $\tau \neq 0$ resulting in Eq. (16) for $\mathbf{k} \rightarrow 0$. Similarly, the leading basis functions for the electric-field induced spin-orbit coupling $\mathbf{g}_{\mathbf{k}}^{II}$ are given by Eq. (B3), with $\tilde{\tau} = 0$ for $\mathcal{G} = D_{6h}$ and C_{6h} ; meanwhile $\tilde{\tau} \neq 0$ for $\mathcal{G} = D_3$. Finally, the leading spin-orbit vector at zero electric field for the point group D_3 is given by $\mathbf{g}_{\mathbf{k}}^I$ in Eq. (B2).